PNAS RESEARCH ARTICLE | PHYSIOLOGY

Trophoblast PR-SET7 dysfunction induces viral mimicry response and necroptosis associated with recurrent miscarriage

Xiaobo Zhou[a,b,1], Yingchun Xu[a,1], Shengnan Ren[a], Ningjie Yang[a], Yang Sun[a], Qibing Yang[a], Yue Zhang[a], Han Cai[a], Wenbo Deng[a], Jingsi Chen[c], Dunjin Chen[c], Bin Cao[a,2], Hongbo Qi[d,2], Haibin Wang[a,2], and Jinhua Lu[a,2]

Edited by Thomas Spencer, University of Missouri, Columbia, MO; received October 6, 2022; accepted May 16, 2023

Recurrent miscarriage (RM) is a distressing pregnancy complication. While the etiology of RM remains unclear, growing evidence has indicated the relevance of trophoblast impairment to the pathogenesis of RM. PR-SET7 is the sole enzyme catalyzing monomethylation of H4K20 (H4K20me1) and has been implicated in many pathophysiological processes. However, how PR-SET7 functions in trophoblasts and its relevance to RM remain unknown. Here, we found that trophoblast-specific loss of *Pr-set7* in mice led to defective trophoblasts, resulting in early embryonic loss. Mechanistic analysis revealed that PR-SET7 deficiency in trophoblasts derepressed endogenous retroviruses (ERVs), leading to double-stranded RNA stress and subsequent viral mimicry, which drove overwhelming interferon response and necroptosis. Further examination discovered that H4K20me1 and H4K20me3 mediated the inhibition of cell-intrinsic expression of ERVs. Importantly, dysregulation of PR-SET7 expression and the corresponding aberrant epigenetic modifications were observed in the placentas of RM. Collectively, our results demonstrate that PR-SET7 acts as an epigenetic transcriptional modulator essential for repressing ERVs in trophoblasts, ensuring normal pregnancy and fetal survival, which sheds new light on potential epigenetic causes contributing to RM.

PR-SET7 | H4K20me1/3 | ERVs | viral mimicry | recurrent miscarriage

Recurrent miscarriage (RM) refers to the failure of two or more clinically diagnosed pregnancies before 20 to 24 weeks of gestation and is experienced by ~2.5% of women trying to conceive (1). Many factors account for the etiology of RM, especially trophoblast dysfunction (1–4). Trophoblasts are the main cellular components of the placenta, which is vital for fetal survival and development during pregnancy (5). The trophoblast subtypes in the placenta are derived from the trophoblast stem cells (TSCs) that undergo extensive proliferation and differentiation. Any disturbance to TSCs could lead to pregnancy disorders, including RM (5).

At each stage of embryonic development, histone modifications play essential roles in chromatin state and gene regulation (6). However, how histone methylations mediate transcriptional regulation at the early developmental stage of extraembryonic trophoblasts still needs further investigation. PR-SET7 is a highly conserved methyltransferase responsible for the monomethylation of H4 at lysine 20 (H4K20me1), which could advance to H4K20me2/3 by SUV4-20H1/2 and be demethylated by PHF8 and hHR23A/B to form H4K20me0, and is implicated in a wide spectrum of physiological and pathological processes (7–9). Experimental evidence has demonstrated the critical roles of PR-SET7 and H4K20me1 during cell cycle progression, DNA repair, and chromosome condensation (10, 11). Mechanistically, H4K20me1 exhibits either a promotive or repressive effect on transcription (12, 13). However, how PR-SET7 functions in trophoblasts remains elusive.

Transposable elements (TEs) are repeated DNA sequences that make up a large fraction of the genome (14). While TE has been confirmed to participate in maintaining chromosome architecture and genomic stability (15, 16), aberrant expression of TEs has emerged as a potential risk factor for a variety of diseases, including cancers, neurological diseases, autoimmune and inflammatory disorders (17, 18), and thus needs to be silenced. DNA methylation, H4K20me3, H3K27me3, and H3K9me3 have been shown to be potential epigenetic modifications responsible for silencing TEs (19–21). However, little is known about the regulation of TEs in trophoblasts, as well as the relevance of dysregulated TEs to pregnancy-related diseases.

Herein, employing in vivo and in vitro models, we demonstrate that PR-SET7-H4K20me1/H4K20me3 inhibits aberrant ERV activation to prevent interferon response and necroptosis in mouse and human trophoblasts. Moreover, we reveal an association between decreased PR-SET7 expression and the occurrence of RM. Together, we define a new epigenetic mechanism via PR-SET7 in trophoblasts potentially contributing to RM.

Significance

The placenta is essential for fetal survival and development during pregnancy. Any disturbance to trophoblasts, the main cellular components of the placenta, could lead to pregnancy disorders. PR-SET7 is the methyltransferase catalyzing monomethylation of H4K20 (H4K20me1), but how it functions in trophoblasts is unclear. In the present work, we demonstrate that PR-SET7-mediated H4K20me1 and H4K20me3 are essential for repressing transcription of endogenous retroviruses (ERVs), preventing double-stranded RNA stress and subsequent overwhelming interferon response and necroptosis in trophoblasts. Importantly, dysregulation of PR-SET7 expression and H4K20me1 is associated with the occurrence of recurrent miscarriage. Our findings reveal an epigenetic mechanism important for the maintenance of trophoblast and placental development potentially underlying the pathogenesis of recurrent miscarriage in women.

The authors declare no competing interest.

This article is a PNAS Direct Submission.

[1]X.Z. and Y.X. contributed equally to this work.

[2]To whom correspondence may be addressed. Email: caobin19@xmu.edu.cn, qihongbocy@gmail.com, haibin.wang@vip.163.com, or jinhua888@126.com.

This article contains supporting information online at https://www.pnas.org/lookup/suppl/doi:10.1073/pnas.2216206120/-/DCSupplemental.

Published June 12, 2023.

Results

Trophoblast-Specific Deletion of *Pr-set7* Leads to Defective Trophoblasts and Pregnancy Loss in Mice. To elucidate the physiological significance of PR-SET7 in trophoblast, we first performed immunohistochemistry (IHC) to examine the spatiotemporal expression pattern of PR-SET7 and H4K20me1 during normal placental development in mice. As illustrated, PR-SET7 and H4K20me1 were expressed in trophoblasts of the extraembryonic ectoderm (ExE), ectoplacental cone (EPC), and chorionic plate (Cp), as well as terminally differentiated trophoblasts from E4.5 to E11.5 (Fig. 1*A* and *SI Appendix*, Fig. S1*A*), suggesting that PR-SET7 might be a crucial regulator of trophoblasts in early placental development.

To depict the phenotype upon *Pr-set7* deletion in vivo, we generated trophoblast-specific *Pr-set7*- knockout (KO) mice ($Pr\text{-}set7^{d/d}$) by crossing $Pr\text{-}set7^{f/f}$ mice with *Elf5-Cre* mice, which specifically functions in trophoblasts (*SI Appendix*, Fig. S1*B*) (22, 23). The Cre-mediated recombination resulted in the deletion of the 7th exon of *Pr-set7* (Fig. 1*B*), which encodes the SET domain necessary for its methyltransferase activity. No $Pr\text{-}set7^{d/d}$ neonates were identified (*SI Appendix*, Table S1), suggesting that *Pr-set7* deletion in trophoblasts leads to embryonic lethality in mice. Consistently, Hematoxylin–Eosin (H&E) staining demonstrated that $Pr\text{-}set7^{d/d}$ embryos exhibited abnormal structures, devoid of ExE and EPC at E5.5-E7.5 (Fig. 1*C*). Immunostaining analyses showed that the expression of eomesodermin (EOMES) and Activator protein 2γ (AP-2γ), markers of trophoblasts in the ExE and EPC, was absent in $Pr\text{-}set7^{d/d}$ embryos, while the epiblast marker octamer-binding transcription factor 4 (OCT4) remained but with abrupt localization in $Pr\text{-}set7^{d/d}$ embryos (Fig. 1*D* and *SI Appendix*, Fig. S1*C*). In addition, the decreased signal of phospho-Histone H3 (pH3) showed impaired proliferation in $Pr\text{-}set7^{d/d}$ embryos (Fig. 1*D*), suggesting trophoblast-specific deletion of *Pr-set7* disturbed embryonic development.

To define the defects of trophoblasts with *Pr-set7* deletion, we examined the $Pr\text{-}set7^{f/f}$ and $Pr\text{-}set7^{d/d}$ embryos at E5.25 before the disappearance of trophoblasts in the ExE. The results of in situ hybridization showed efficient deletion of *Pr-set7* in the ExE of $Pr\text{-}set7^{d/d}$ embryos (*SI Appendix*, Fig. S1*D*). Accordingly, H4K20me1-positive trophoblast cells were largely decreased in $Pr\text{-}set7^{d/d}$ ExE (Fig. 1*E*). Immunostaining of phospho-Histone H2A.X (Ser139) (γH2AX), a marker of DNA double-strand breaks (DSB) foci and DNA damage, revealed massive DNA damage in trophoblasts resident in the ExE of $Pr\text{-}set7^{d/d}$ embryos (Fig. 1*E*). Together, these data suggest that trophoblast-specific deletion of *Pr-set7* impairs H4K20 methylation and leads to defective trophoblasts and pregnancy loss.

PR-SET7 Deficiency Induces Genome Instability in Trophoblasts. To further confirm the significance of PR-SET7 in trophoblasts, we derived mouse TSCs (mTSCs) from $Pr\text{-}set7^{f/f}$ blastocysts and human TSCs (hTSCs) from the first-trimester placental villous tissues. The immunofluorescent and quantitative real-time PCR (qRT-PCR) analysis of marker genes confirmed the stemness and differentiation abilities of mTSCs and hTSCs, respectively (*SI Appendix*, Fig. S2). We deleted *Pr-set7* by introducing exogenous doxycycline (Dox) induced PiggyBac-Cre plasmid into $Pr\text{-}set7^{f/f}$ mTSCs (Fig. 2*A*). Cell proliferation was significantly blunted upon *Pr-set7* deletion in mTSCs (Fig. 2*B*). Flow cytometric analysis of cell cycle progression revealed that increased ratio of *Pr-set7*-depleted mTSCs were assigned to the G0/G1 phase (Fig. 2*C*), consistent with the observation of decreased 5-ethynyl-2′-deoxyuridine (EdU) incorporations in mTSCs upon *Pr-set7* deletion (Fig. 2*D*). Furthermore, the number of γH2AX-positive trophoblasts was significantly increased in *Pr-set7*-deficient mTSCs (Fig. 2*D*). In addition, mTSCs treated with UNC0379, a selective substrate-competitive inhibitor of PR-SET7, displayed a similar phenotype as that observed in *Pr-set7*-depleted mTSCs (*SI Appendix*, Fig. S3 *A*–*C*). These findings imply that PR-SET7 is

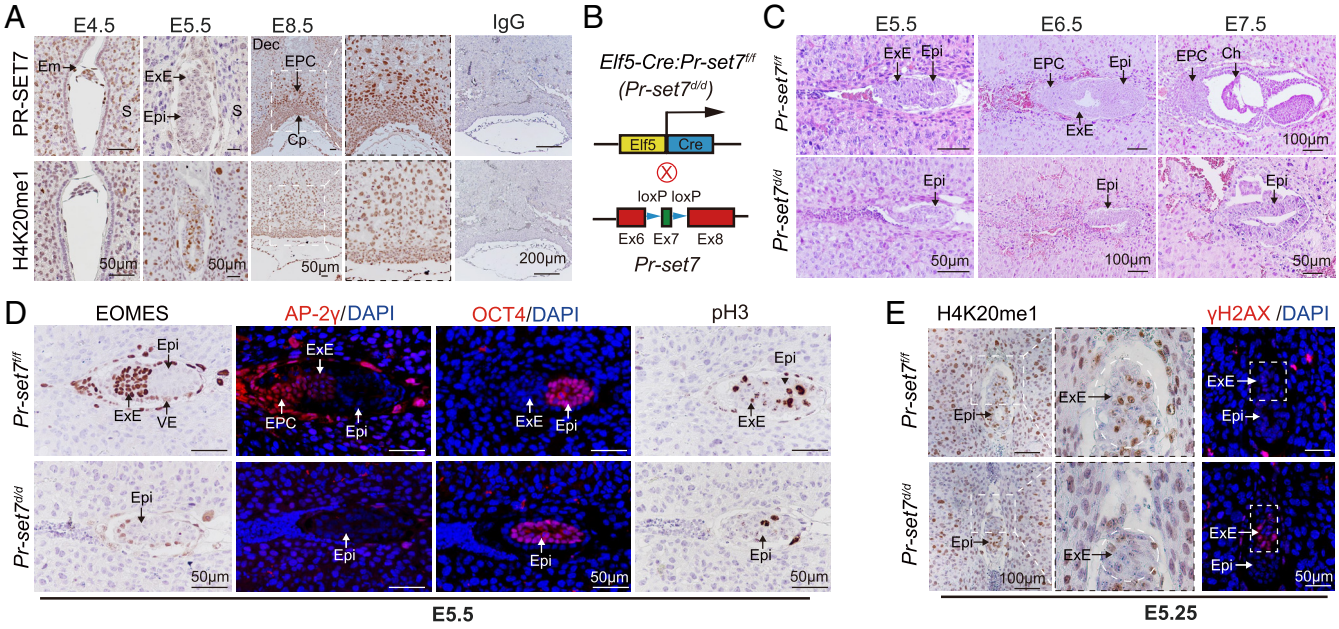

Fig. 1. Trophoblast-specific deletion of *Pr-set7* leads to pregnancy loss in mice. (*A*) Immunohistochemical analysis of PR-SET7 and H4K20me1 expression at E4.5–E8.5 during normal placental development. (*B*) The strategy for generating mice with trophoblast-specific deletion of *Pr-set7* ($Pr\text{-}set7^{d/d}$). (*C*) H&E staining of implantation sites of $Pr\text{-}set7^{f/f}$ and $Pr\text{-}set7^{d/d}$ mice at E5.5–E7.5. (*D*) Representative Immunostaining images of EOMES, AP-2γ, OCT4, and pH3 in $Pr\text{-}set7^{f/f}$ and $Pr\text{-}set7^{d/d}$ embryos at E5.5. (*E*) Immunostaining images of H4K20me1 and γH2AX in $Pr\text{-}set7^{f/f}$ and $Pr\text{-}set7^{f/f}$ embryos at E5.25. Images in *A* and *C*–*E* are representative of at least two or three independent experiments, respectively. Em, embryo; ExE, extraembryonic ectoderm; Epi, epiblast; EPC, ectoplacental cone; Ch, chorion; Cp, chorionic plate; S, uterine stromal cells; VE, visceral endoderm.

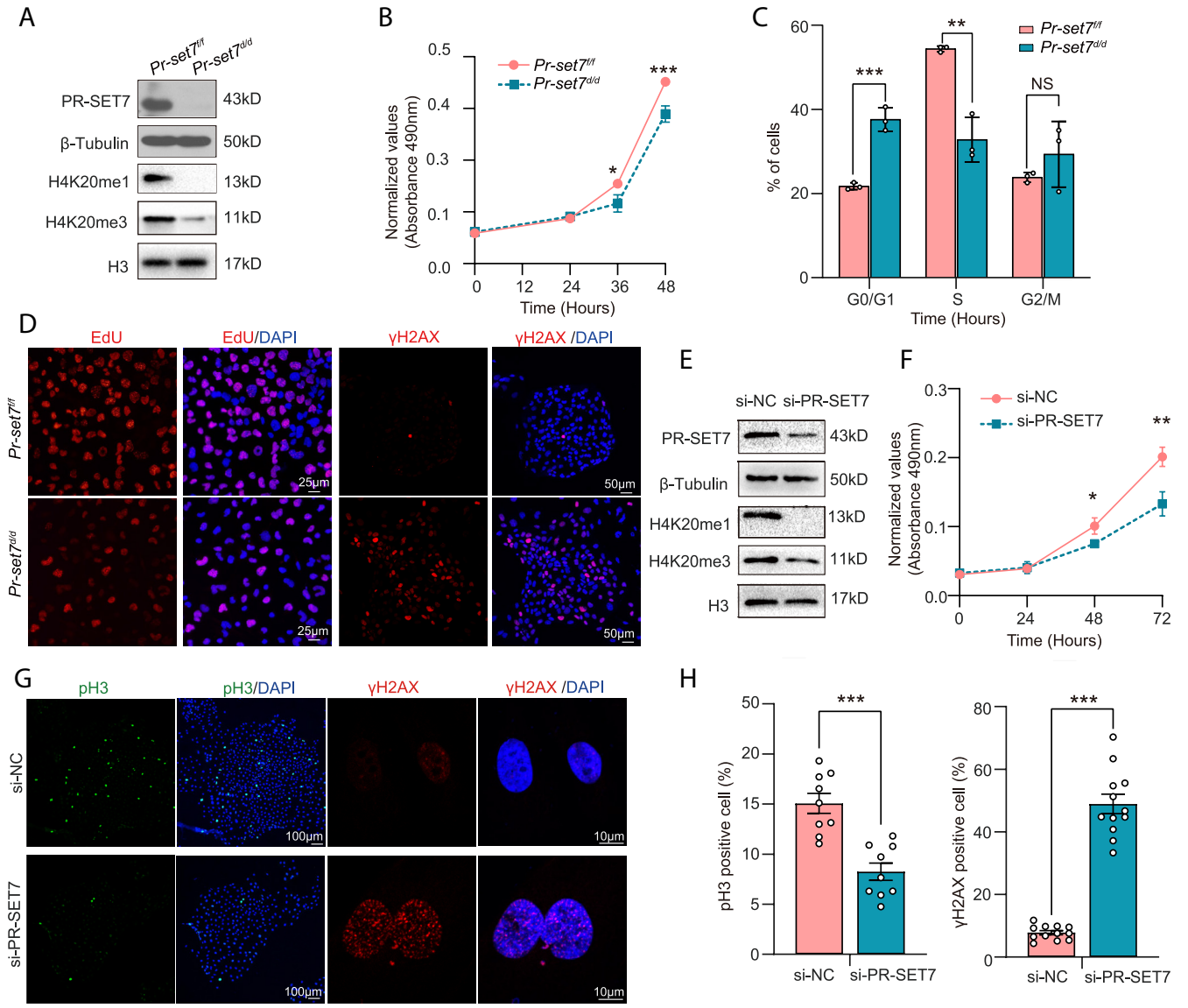

Fig. 2. PR-Set7 deficiency induces genome instability in TSCs. (*A*) Immunoblot analysis of PR-SET7, H4K20me1, and H4K20me3 in mTSCs treated with or without Dox for 48 h (*Pr-set7*$^{d/d}$ and *Pr-set7*$^{f/f}$). β-Tubulin and H3 were used as loading controls. n = 3. (*B*) The MTS assay showed an impaired proliferation of mTSCs upon *Pr-set7* knockout. n = 3. (*C*) FACS analysis revealed significant cell cycle arrest in mTSCs treated with Dox for 24 h (*Pr-set7*$^{d/d}$). n = 3. (*D*) Immunofluorescence analysis of EdU and γH2AX in mTSCs treated with or without Dox for 24 h (*Pr-set7*$^{d/d}$ and *Pr-set7*$^{f/f}$). (*E*) Immunoblot analysis showed decreased levels of PR-SET7, H4K20me1, and H4K20me3 in the presence of si-PR-SET7 for 48 h. β-Tubulin and H3 were used as loading controls. n = 3. (*F*) The MTS assay of hTSCs transfected with si-NC or si-PR-SET7 for indicated hours. n = 3. (*G*) Immunofluorescence analysis of γH2AX and pH3 in hTSCs transfected with si-NC or si-PR-SET7 for 48 h. (*H*) The quantitative results of *G*. Images in *D* and *G* are representative of at least three independent experiments. In *B*, *C*, *F*, and *H*, Two-tailed unpaired Student's t test. **P* < 0.05, ***P* < 0.01, ****P* < 0.001.

essential for trophoblast maintenance at the early stages of mouse placental development.

In addition, upon abrogation of *PR-SET7* by siRNAs in hTSCs (Fig. 2*E* and *SI Appendix*, Fig. S3 *D* and *E*), cell proliferation was significantly abolished (Fig. 2*F*), which was further confirmed by the decreased ratio of pH3-positive trophoblasts (Fig. 2 *G* and *H*). Moreover, *PR-SET7* knockdown (KD) in hTSCs led to massive DNA damage, as shown by the increased ratio of γH2AX-positive cells (Fig. 2 *G* and *H*). These findings further demonstrate that PR-SET7 is essential for the genome stability and maintenance of the TSC population during early placental development.

Ablation of PR-SET7 Results in Necroptosis in Trophoblasts. To further investigate the molecular mechanisms underlying PR-SET7 deficiency in trophoblasts, we performed whole-transcriptome RNA sequencing (RNA-seq) comparing the control and PR-SET7-deficient TSCs in both mouse and human. We observed 972 upregulated genes and 775 downregulated genes in mTSCs upon *Pr-set7* knockout (*SI Appendix*, Fig. S4*A* and Dataset S1, cutoff: fold change > 1.5, adjusted *P* value < 0.05), as well as 528 downregulated and 1,025 upregulated genes in hTSCs treated with si-PR-SET7 (*SI Appendix*, Fig. S4*C* and Dataset S2, cutoff: fold change > 1.5, adjusted *P* value < 0.05). Genes associated with DNA repair were downregulated in PR-SET7-depleted cells (*SI Appendix*, Fig. S4 *B* and *D*). Gene Set Enrichment Analysis (GSEA) revealed significant enrichment of genes involved in apoptosis and the p53 pathway (Fig. 3 *A* and *B*), consistent with previous observations showing that PR-SET7 is a key regulator of cell apoptosis and DNA repair (24). Furthermore, the genes associated with cell death were also increased upon PR-SET7 deficiency (Fig. 3*C* and *SI Appendix*, Fig. S4*E*). Upregulated expression of genes related to cell death, including *glutathione*

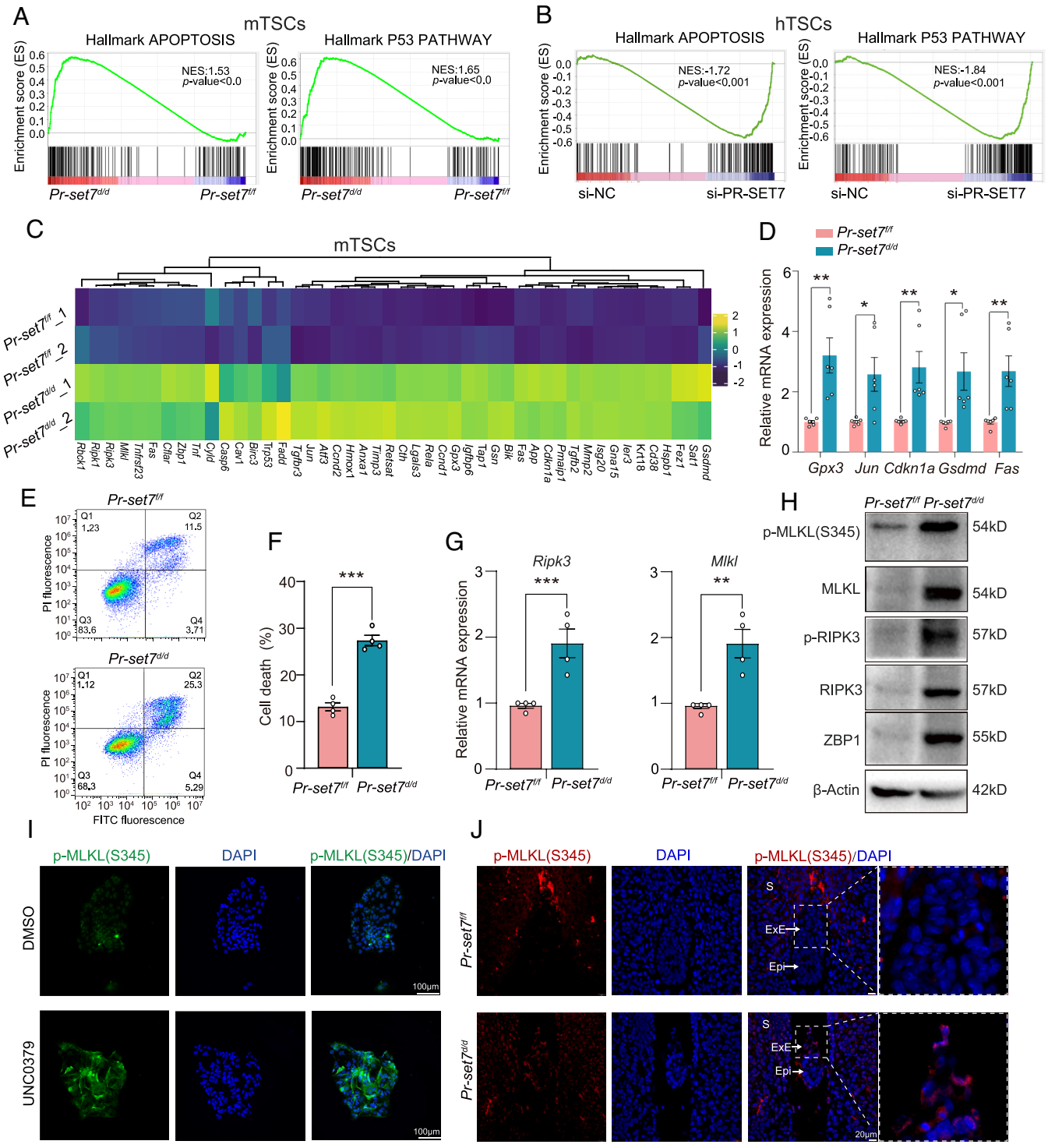

Fig. 3. *PR-SET7* deficiency results in necroptosis in TSCs. (*A* and *B*) GSEA shows the enrichment of genes involved in apoptosis and the p53 pathway in TSCs with PR-SET7 deletion in both mice (*A*) and humans (*B*). NES, normalized enrichment score. (*C*) Heatmap showing upregulation of genes involved in cell death upon *Pr-set7* deletion in mTSCs. (*D*) qRT-PCR confirmed the upregulation of representative genes of cell death. n = 6. (*E* and *F*) FACS analysis revealed increased cell death in *Pr-set7*$^{d/d}$ mTSCs. Two-tailed unpaired Student's *t* test, ***$P < 0.001$. n = 4. (*G*) qRT-PCR confirmed increased expression of *Ripk3* and *Mlkl*. n = 4. (*H*) Immunoblots of p-MLKL(S345), MLKL, p-RIPK3, RIPK3, and ZBP1 in *Pr-set7*$^{d/d}$ versus *Pr-set7*$^{f/f}$ mTSCs. β-Actin was used as a loading control. n = 3. (*I* and *J*) Immunostaining of p-MLKL(S345) in mTSCs treated with or without UNC0379 for 48 h (*I*) and in *Pr-set7*$^{f/f}$ and *Pr-set7*$^{d/d}$ embryos at E5.25 (*J*). ExE, extraembryonic ectoderm; Epi, epiblast; S, uterine stromal cells. The images are representative of at least three independent experiments. In *D* and *G*, the values are normalized to *Gapdh* and indicated as the mean ± SEM. Two-tailed unpaired Student's *t* test, *$P < 0.05$, **$P < 0.01$, ***$P < 0.001$.

peroxidase 3 (*Gpx3*), *Jun*, *Cdkn1a*, *gasdermin D* (*Gsdmd*), and *Fas* in *Pr-set7*-KO mTSCs was further confirmed by qRT-PCR analysis (Fig. 3*D*). We also revealed significantly increased expression of cell death related genes in *PR-SET7*-KD hTSCs (*SI Appendix*, Fig. S4*F*). Fluorescence-activated cell sorting (FACS) analysis confirmed the increased cell death in mTSCs with *Pr-set7* deletion (Fig. 3 *E* and *F*). Specifically, necroptosis was activated in *Pr-set7*-deleted mTSCs as shown by the increased expression of *mixed lineage kinase domain-like* (*Mlkl*) and *receptor-interacting serine-threonine kinase 3* (*Ripk3*) (Fig. 3 *C* and *G*). We also found

an increased expression of p-RIPK3, RIPK3, p-MLKL(S345), MLKL, and Z-DNA-binding protein 1 (ZBP1) in *Pr-set7*$^{d/d}$ mTSCs (Fig. 3*H*), indicating the occurrence of necroptosis upon *Pr-set7* ablation. Besides, UNC0379-treated mTSCs also showed increased expression of p-MLKL(S345) (Fig. 3*I*). Consistently, immunostaining of p-MLKL(S345) revealed increased p-MLKL(S345) in trophoblasts resident in the ExE of *Pr-set7*$^{d/d}$ embryos at E5.25 (Fig. 3*J*), further demonstrating the connections between PR-SET7 deficiency and necroptosis. These results collectively indicate that necroptosis occurs in trophoblasts in the absence of PR-SET7.

PR-SET7 Loss Induces Interferon Response in Trophoblasts. It was intriguing to notice that the differentially expressed genes (DEGs) upon *PR-SET7* KD were enriched in signaling pathways of bacterial origin, response to lipopolysaccharide, leukocyte migration, and T cell activation (Fig. 4*A*). This notion was confirmed by the GSEA analysis, showing that allograft rejection, inflammatory response, interferon-alpha response, and tumor necrosis factor alpha (TNFα) signaling via nuclear factor kappa B (NF-κB) pathway were enriched in PR-SET7-deficient cells (Fig. 4*B*). Moreover, many genes involved in the inflammatory and interferon response were upregulated (Fig. 4*C*). *Interferon-stimulated gene 15* (*ISG15*),

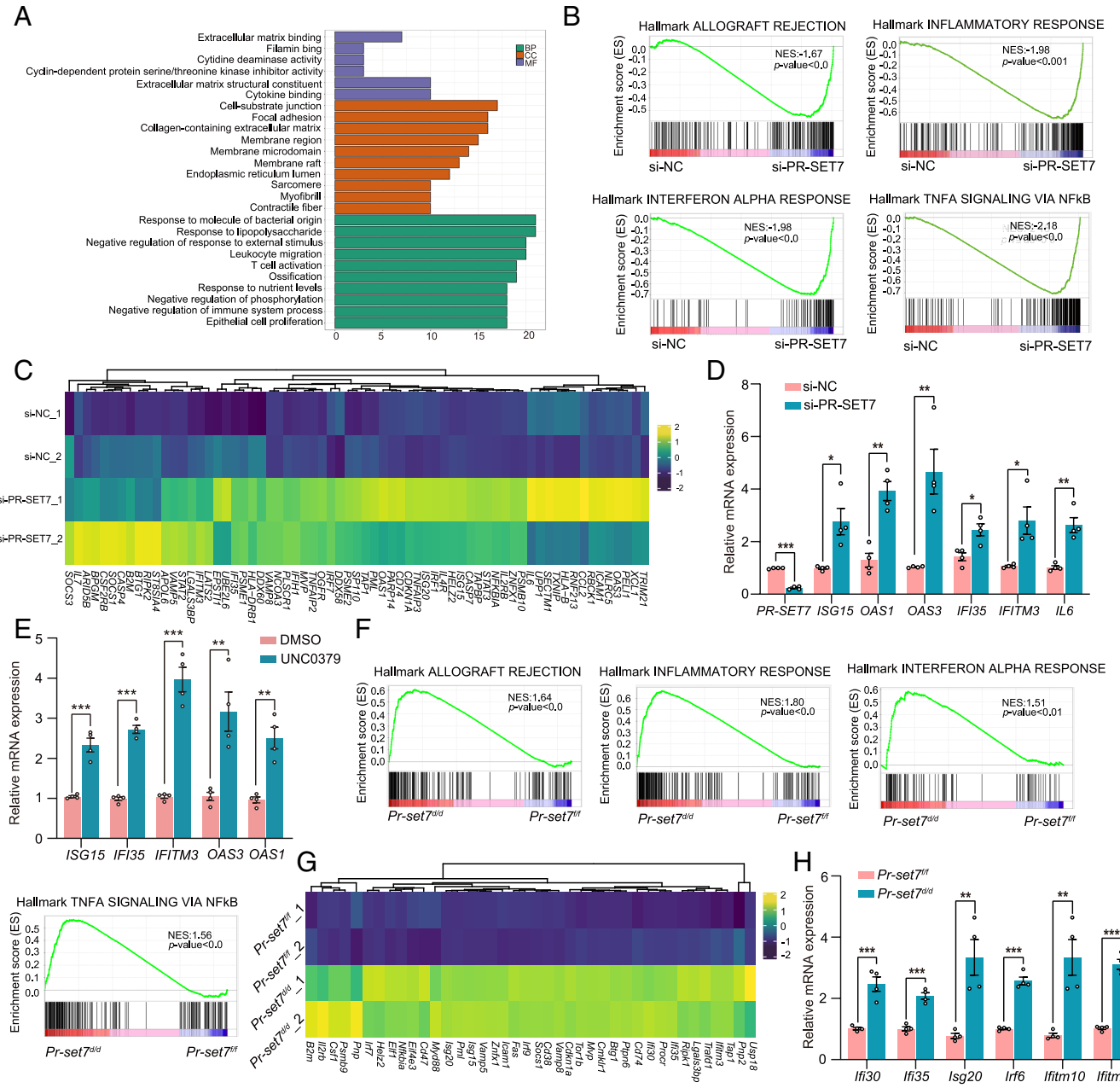

Fig. 4. *PR-SET7* deletion activates interferon response in TSCs. (*A*) Gene ontology (GO) analysis of the DEGs in *PR-SET7*-knockdown versus control hTSCs. BP, Biological Process; CC, Cellular Component; MF, Molecular Function. (*B*) GSEA reveals the changes in the indicated gene signatures in hTSCs upon PR-SET7 deletion. (*C*) Heatmap showing the upregulation of genes involved in inflammatory response and interferon response in hTSCs with *PR-SET7* knockdown. (*D* and *E*) qRT-PCR confirmed the upregulation of representative genes of the inflammatory response and interferon response in hTSCs with *PR-SET7* knockdown (*D*) and treated with UNC0779 (*E*), respectively. (*F*) GSEA reveals the changes in the indicated gene signatures in mTSCs upon *Pr-set7* knockout. (*G*) Heatmap showing the upregulation of genes involved in the interferon response in *Pr-set7*$^{d/d}$ mTSCs. (*H*) qRT-PCR confirmed the upregulation of representative genes related to interferon response signaling pathway. In *D*, *E*, and *H*, the values are normalized to *Gapdh* and indicated as the mean ± SEM. Two-tailed unpaired Student's *t* test, **P* < 0.05, ***P* < 0.01, ****P* < 0.001. n = 4.

2′-5′-Oligoadenylate synthetase 1 (*OAS1*), *OAS3*, *Interferon-induced protein 35* (*IFI35*), *Interferon-induced transmembrane protein 3* (*IFITM3*), and *Interleukin 6* (*IL6*) were significantly induced in *PR-SET7*-KD hTSCs (Fig. 4 *C* and *D*). Consistently, UNC0379 treatment also induced upregulated expressions of *ISG15, IFI35, IFITM3, OAS3,* and *OAS1* (Fig. 4*E*). Besides, the gene sets in *Pr-set7*$^{d/d}$ mTSCs (Fig. 4*F*) were similar to that in hTSCs. The expression of interferon-stimulated genes, like *interferon gamma inducible protein 30* (*Ifi30*), *Ifi35*, *Isg20*, *interferon regulatory factor 6* (*Irf6*), *Ifitm10*, and *Ifitm3* was similarly upregulated in *Pr-set7*-depleted mTSCs (Fig. 4 *G* and *H*). These results demonstrate that PR-SET7 deficiency induces an aberrant interferon response.

PR-SET7-H4K20me1 Represses Interferon-Related Genes Indirectly. We subsequently explored the mechanisms underlying the enhanced expression of ISGs involved in interferon response caused by PR-SET7 deficiency. PR-SET7 has been implicated in both transcriptional activation and repression, and the transcriptional role of PR-SET7 is mainly mediated via its methyltransferase activity targeting H4K20me1 (11). In addition to functioning directly, H4K20me1 also acts as the substrate for H4K20me3, which is required for heterochromatin maintenance. Since H4K20me1 and H4K20me3 decreased when PR-SET7 was deleted in TSCs (Fig. 2 *A* and *E*), we examined the genomic distribution of H4K20me1 and H4K20me3 by chromatin immunoprecipitation followed by sequencing (ChIP-Seq) to reveal their relevance to gene expression in TSCs. Compared with the main promoter enrichment of tri-methylation at the 4th lysine residue of the histone H3 protein (H3K4me3), H4K20me1 was enriched toward the promoters, gene body regions, and distal intergenic regions, and H4K20me3 was mainly enriched toward the gene body and distal intergenic regions (Fig. 5 *A*–*C*). Combined with the RNA-seq data, we found that H3K4me3 was highly enriched in the promoters of the expressed genes (FPKM ≥ 1) (Fig. 5*C*). While H4K20me1 was mainly enriched in the gene body of the expressed genes (FPKM ≥ 1), it was also enriched in the promoters of nonexpressed genes (FPKM < 1) (Fig. 5*C*), suggesting that H4K20me1 might function in both transcriptional activation and repression in TSCs. Via comparing the enrichment of H4K20me1 on DEGs, we found that H4K20me1 was enriched on both upregulated and downregulated genes, with the upregulated genes possessing more H4K20me1 enrichment than the downregulated genes (Fig. 5*D*), indicating that PR-SET7-H4K20me1 exerts both promotive and repressive effects on transcription in TSCs.

To test the possibility that H4K20me1 might repress the expression of ISGs directly, we further integrated and analyzed the ChIP-seq and RNA-seq datasets in TSCs, and observed 406 genes associated with angiogenesis, signal transduction, and cell migration were both upregulated upon *PR-SET7* deletion and targeted by H4K20me1 (Fig. 5 *E* and *F*), while the upregulated ISGs, such as *OAS3, IL6, ISG15*, *IFITM3*, *toll-like receptor 3* (*TLR3*), *TLR7*, *apolipoprotein B mRNA-editing enzyme catalytic subunit 3C* (*APOBEC3C*), and *APOBEC3G* were not targeted directly by H4K20me1 (Fig. 5*G*). This observation suggests that ablation of PR-SET7-H4K20me1 augments the expression of ISGs indirectly.

In mTSCs, the genomic distribution of H4K20me1 and H4K20me3 by ChIP-Seq showed similar patterns to that in hTSCs (*SI Appendix*, Fig. S5 *A* and *B*). The ChIP-seq data of H3K4me3 showed that the genes bound by H3K4me3 had elevated H3K4me3 levels upon *Pr-set7* KO, indicating the occurrence of derepression (*SI Appendix*, Fig. S5 *C* and *D*). However, the ISGs, such as *Tlr5, Ifi30, Irf6*, *Ifitm3*, *Mlkl*, *Gsdmd,* and *serpin family B member 9* (*Serpinb9*), were not targeted directly by H4K20me1 (Fig. 5*H*). These findings further confirm that PR-SET7 and H4K20me1 regulate interferon-related genes indirectly. In addition, since *Mlkl* is also the necroptosis executioner, necroptosis is also likely modulated indirectly by PR-SET7 and H4K20me1.

PR-SET7 Deficiency Induces ERV Expression and Aberrant Cytoplasmic Accumulation of Double-Stranded RNAs (dsRNAs). It has been reported that virus sensing is implicated in triggering inflammatory caspases, innate and adaptive immune responses, and cell death to disrupt the replicative niche necessary for intracellular pathogens (25, 26). Since trophoblast PR-SET7 deficiency induces an obviously upregulated gene expressions involved in interferon response and necroptosis, we speculated that this respective aberrant expression profile in PR-SET7-deficient TSCs may be due to intracellular derepression of ERVs and accumulation of dsRNAs, which have been shown to induce aberrant viral mimicry interferon response, and necroptosis. Indeed, Kyoto Encyclopedia of Genes and Genomes (KEGG) analysis revealed that the upregulated genes were enriched in pathways involved in multiple viral infections in both hTSCs and mTSCs (Fig. 6*A* and *SI Appendix*, Fig. S6 *A* and *B*). RNA-seq, which determines the differentially expressed TEs in a genome-wide manner, revealed that the expression of long terminal repeats (LTRs), i.e., ERVs, was upregulated significantly in *PR-SET7*-deficient TSCs (Fig. 6*B*, *SI Appendix*, Fig. S6*C*, and Dataset S3). The analysis of ChIP-seq data revealed widespread binding of H4K20me1 and H4K20me3 to ERVs (Fig. 6*C*). By integrating H4K20me1 ChIP-seq data with ERV elements expression, we observed an inverse correlation between the binding of H4K20me1 and the expression of ERVs (Fig. 6*D*), indicating a potential repressive role of H4K20me1 on ERV expression. Furthermore, H4K20me1 and H4K20me3 were mainly enriched in the gene bodies of the ERVs (Fig. 6 *C* and *E*). For example, H4K20me1 and H4K20me3 were directly bound to the gene body of HERVH-int: ERV1: LTR (Fig. 6 *F* and *G*). We then used the J2 antibody, which specifically detects dsRNAs, to explore whether the upregulated ERV transcription would result in increased dsRNA formation. Indeed, qRT-PCR analysis of ERVs captured by J2 pull-down assay showed that the upregulated ERVs in *PR-SET7*-KD hTSCs formed more dsRNA, which was confirmed by the immunostaining of J2 antibody (Fig. 6 *H* and *I*). Meanwhile, the dot-blot analysis indicated increased dsRNA abundance in *Pr-set7*-KO mTSCs (*SI Appendix*, Fig. S6*D*). These data demonstrate that PR-SET7 deficiency induces the expression of ERVs and aberrant cytoplasmic accumulation of dsRNAs.

Endosomal and cytosolic RNA sensors detect intracellular dsRNAs, activating interferon response and cell death (27). We found that the dsRNA sensors *TLR3, TLR7,* and *melanoma differentiation-associated protein 5* (*MDA5*) were upregulated in *PR-SET7*-KD hTSCs (Fig. 6*J*). Moreover, RNA sensors were also upregulated in *Pr-set7*-KO mTSCs (Fig. 3 *C* and *H* and *SI Appendix*, Fig. S6*E*). While the expression of mitochondrial antiviral signaling protein (MAVS), the downstream signal transducer of MDA5, increased in *PR-SET7*-KD hTSCs, MAVS knockdown failed to rescue the disturbed ISG expression induced by *PR-SET7* KD (*SI Appendix*, Fig. S7 *A* and *B*). However, the inhibition of the dsRNA sensor TLR3 with its inhibitor TLR3-IN-1 partially decreased the increased expression of *ISG15* and *IFI35* in *PR-SET7*-KD hTSCs (Fig. 6*K*), suggesting the involvement of dsRNA-TLR3 signaling in the interferon response induced by *PR-SET7* deficiency. Accordingly, the downstream signaling of dsRNA-TLR3, shown by the upregulation of p-IRF3 and the enhanced expression of *IFNα*, *IFNλ1* and *IFNλ2*, was increased significantly in *PR-SET7*-KD hTSCs (*SI Appendix*, Fig. S8 *A* and *B*).

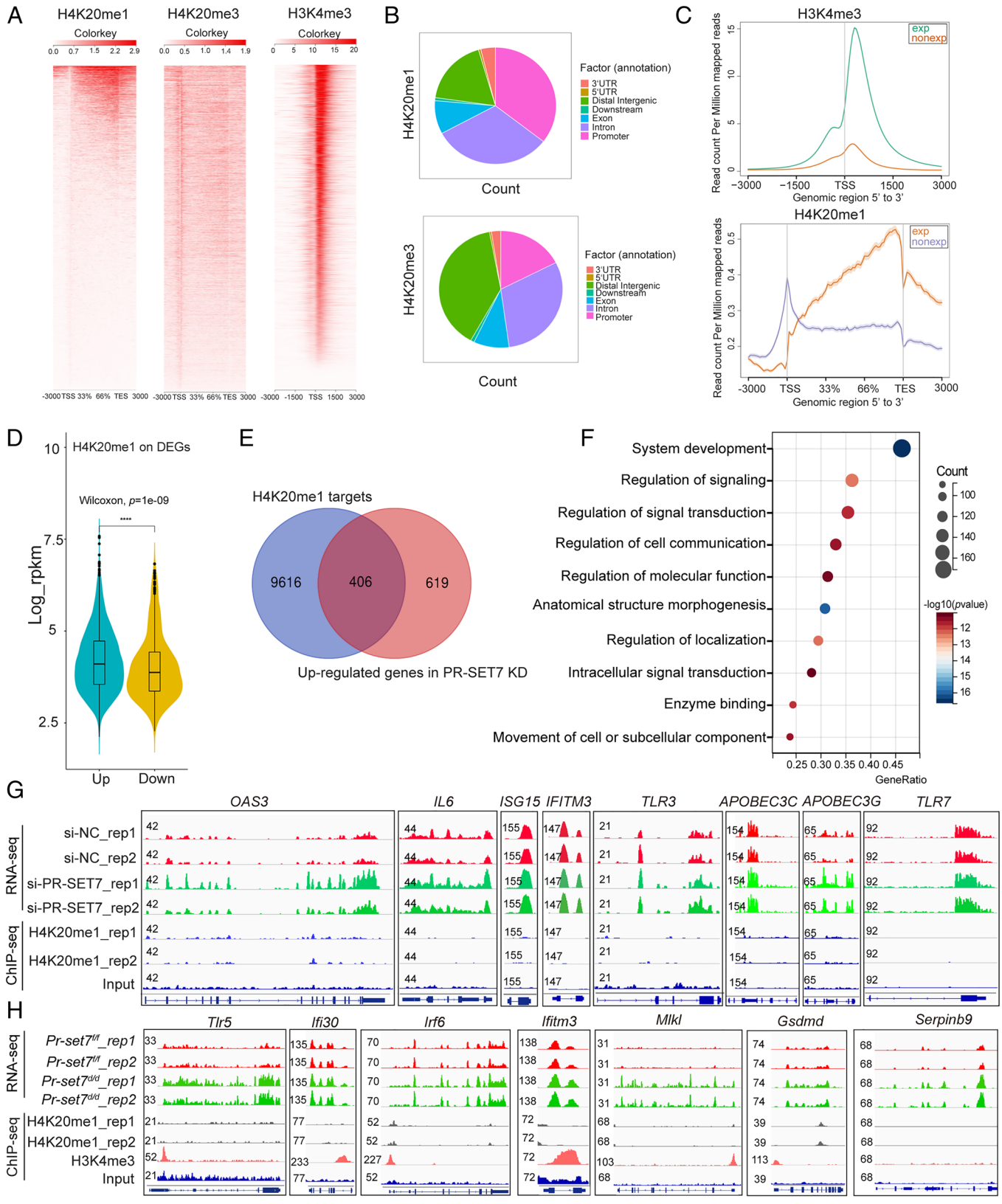

Fig. 5. PR-SET7-H4K20me1 represses interferon-related genes indirectly in TSCs. (*A*) Heatmap representation of H4K20me1, H4K20me3, and H3K4me3 ChIP-seq tag density within 3,000 bp around TSS in hTSCs. (*B*) Genomic read distributions of H4K20me1 and H4K20me3 binding sites in hTSCs. (*C*) Average ChIP-seq tag density plots of H3K4me3 (*Upper*) and H4K20me1 (*Lower*) on highly expressed or non-expressed genes in the region −3,000 bp upstream of TSS and 3,000 bp downstream of TES. (*D*) Average ChIP-seq read density of H4K20me1 on DEGs from RNA-seq data of hTSCs. (*E* and *F*) Venn diagram showing the overlap of H4K20me1 targets and upregulated genes induced by si-PR-SET7 (*E*) and GO analysis of the common genes (*F*) in hTSCs. (*G*) Genome browser view of normalized RNA-seq tracks and ChIP-seq signals of H4K20me1 at the interferon signaling-associated gene locus. (*H*) Representative RNA-seq tracks, the ChIP-seq signals of H4K20me1 and H3K4me3 at the ISGs locus. TSS, Transcription Start Site; TES, Transcription End Site.

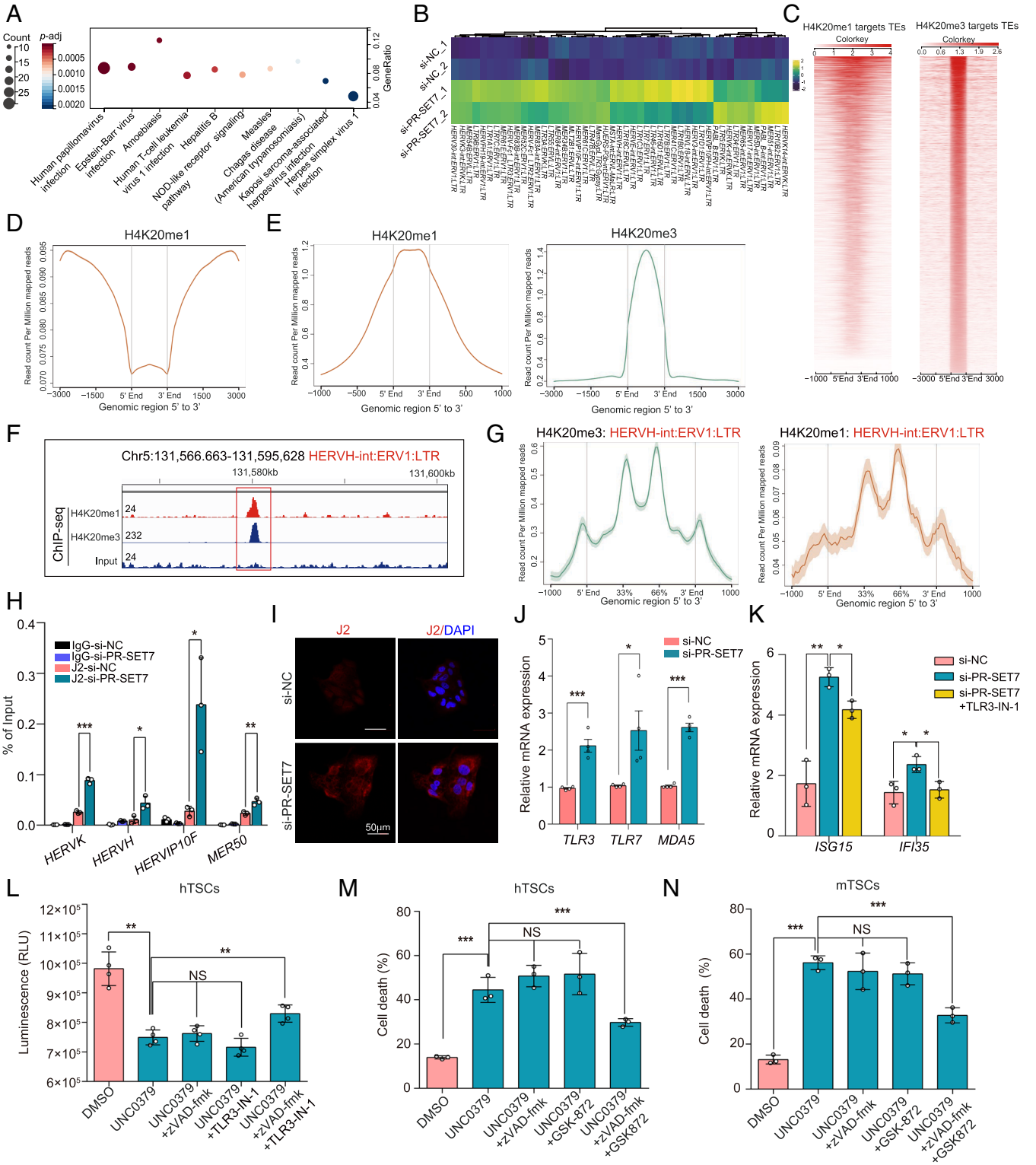

Fig. 6. PR-SET7 deficiency induces ERV expression and dsRNA formation in TSCs. (*A*) KEGG enrichment analysis showed that the upregulated genes were associated with multiple viral infection responses. (*B*) Heatmap showing the differential expression of ERVs upon *PR-SET7* KD in hTSCs. (*C*) Heatmap representation of ChIP-seq tag density of H4K20me1 and H4K20me3 binding to TEs. (*D*) The analysis of ChIP-seq data and ERV transcripts expression revealed an inverse correlation between H4K20me1 binding and ERV expression. (*E*) Average ChIP-seq tag density plots of H4K20me1 and H4K20me3 on ERVs in the region upstream of TSS to downstream of TES. (*F* and *G*) Representative UCSC tracks and ChIP-seq analysis of H4K20me3 and H4K20me1 at HERVH-int: ERV1: LTR locus. (*H*) qRT-PCR analysis of the ERVs captured by J2 antibody in the pull-down assay. (*I*) Immunostaining of J2 in hTSCs transfected with si-NC or si-PR-SET7 for 48 h. n = 3. (*J*) qRT-PCR analysis revealed the upregulation of dsRNA sensors in hTSCs treated with si-PR-SET7. n = 4. (*K*) qRT-PCR analysis revealed the increased expression of interferon response genes in hTSCs treated with si-PR-SET7 was partially reversed by TLR3 inhibitor TLR3-IN-1. n = 3. (*L*) The analysis of cell viability in hTSCs treated with UNC0379 (2.5 μM), with or without zVAD-fmk (10 mM) or/and TLR3-IN-1(20 μM). (*M* and *N*) The analysis of cell death in hTSCs (*M*) and mTSCs (*N*) treated with UNC0379 (5 μM in mTSCs) for 48 h with or without zVAD-fmk (10 mM) or/and GSK872 (2 mM). Two-tailed unpaired Student's *t* test, NS, no significance, ***$P < 0.001$. In *J* and *K*, the values are normalized to *GAPDH* and indicated as the mean ± SEM. Two-tailed unpaired Student's *t* test, *$P < 0.05$, **$P < 0.01$, ***$P < 0.001$.

Moreover, TLR3 activation by dsRNA has also been reported to trigger cell death, including necroptosis (28, 29). To investigate whether the inhibition of TLR3 could attenuate necroptosis in PR-SET7-deficient hTSCs, TLR3-IN-1 was used in the presence of zVAD-fmk, an inhibitor of pan-caspase, since apoptosis also occurred in PR-SET7-deficient hTSCs. The significantly increased cell viability of PR-SET7-deficient TSCs with the cotreatment of TLR3-IN-1 and zVAD-fmk (Fig. 6*L*) demonstrated the involvement of dsRNA-TLR3 signaling in necroptosis upon PR-SET7 deficiency in trophoblasts. To further address the involvement of necroptosis in the trophoblast defects caused by PR-SET7 deficiency, the RIPK3 inhibitor GSK872 was applied in the presence of zVAD-fmk. The significantly blunted cell death in the presence of zVAD-fmk and GSK872 cotreatment (Fig. 6 *M* and *N*) confirmed the occurrence of necroptosis in the absence of PR-SET7. Taken together, these findings indicate that the trophoblast defects caused by PR-SET7 deficiency could be partially explained by ERVs-dsRNA-TLR3-triggered viral mimicry response and necroptosis.

Decreased Expression of PR-SET7 Is Associated with RM. To investigate the potential contribution of PR-SET7 and H4K20me1 to pregnancy maintenance, we compared PR-SET7 expression and H4K20me1 in placental villous tissues from terminated normal pregnancies and patients with RM. We found that PR-SET7 was localized mainly in cytotrophoblasts (CTs), and H4K20me1 was expressed in both CTs and syncytiotrophoblasts of the placental villi (Fig. 7*A*). While the levels of histone methylation H3K27me3 and H3K9me3 did not show apparent difference (*SI Appendix*, Fig. S9), H4K20me1 and PR-SET7 were significantly downregulated in the villous tissues of RM (Fig. 7 *B* and *C*). These findings indicate a close correlation between dysregulated PR-SET7-H4K20me1 and the occurrence of RM. Immunostaining analysis verified the decreased Ki-67 and MCM2-positive CTs in the villi of RM, which implies an impaired proliferation activity (Fig. 7 *D* and *E*). More importantly, we found augmented γH2AX-positive cells (Fig. 7 *D* and *E*), increased ERV expression (Fig. 7*F*), and higher levels of dsRNA (J2 signal) formation in the villous trophoblast of RM pregnancies (Fig. 7 *G* and *H*). Accordingly, we found enhanced expression of p-MLKL(S358) in villous CTs of RM pregnancies (Fig. 7 *G* and *I*). Altogether, our findings of association of abnormal PR-SET7 and H4K20me1 expressions with aberrantly increased ERV and dsRNA levels in human placentas, indicate that PR-SET7 dysfunction is a potentially important contributor to the pathogenesis of RM.

Discussion

RM is a highly heterogeneous pregnancy disorder relevant to various nosogenesis, among which the involvement of PR-SET7 in placental development and its relevance to RM remain elusive. Employing multiple approaches, we provide herein pathophysiological and genetic evidence that PR-SET7-mediated histone methylation is essential for maintaining chromatin status and repressing ERV transcription to prevent the cell-intrinsic activation of interferon response and necroptosis in trophoblasts. The pivotal functions of PR-SET7 in transcriptional repression ensure the survival of trophoblasts, whereas the dysfunction of PR-SET7 might contribute to the pathogenesis of RM (Fig. 8), highlighting that PR-SET7 is indispensable for placental development and the maintenance of pregnancy.

Normal placental development requires tightly regulated proliferation and differentiation of trophoblasts, while abnormal self-renewal, differentiation, and cell death could lead to pregnancy disorders such as pre-eclampsia and preterm birth (30). Existing investigations have uncovered excessive apoptosis of trophoblasts in RM (31, 32). Our study demonstrates that *PR-SET7*-deficient TSCs show different types of cell death, since cotreatment of *PR-SET7*-deficient TSCs with the inhibitors of apoptosis and necroptosis only partially rescued the cell death. The occurrence of necroptosis in TSCs upon PR-SET7 deficiency in culture is consistent with in vivo status, since increased p-MLKL(S358) expression was noted in villous CTs from RM pregnancies. The factors responsible for the induction of necroptosis are various (27). While the prototypical model of necroptosis is induced by the cytokine TNF (33), it has been shown that type I interferons cause RIPK3-dependent necroptosis in macrophages in the presence of *Salmonella typhimurium* infection (34). Moreover, ZBP1, acting as a nucleotide sensor, has been reported to trigger necroptosis via interacting with RIPK3 (20, 35). In addition, necroptosis can also occur downstream of TLRs (27). In the present work, we demonstrate that PR-SET7 inactivation elicits the accumulation of dsRNAs and the expression of dsRNA sensors, such as ZBP1 and TLRs. We further provide evidence that TLR3 is involved in the occurrence of necroptosis in trophoblasts triggered by PR-SET7 deficiency. Since pathways associated with interferon-alpha response and TNFα signaling via NF-κB were enriched in PR-SET7-deficient TSCs, there might be alternative mechanisms independent of TLR3 contributing to the occurrence of necroptosis in TSCs in the absence of PR-SET7, which warrants further investigation.

Although TEs have the epithet "junk DNA," they benefit their host in some circumstances. It has been shown that ERVs can create species-specific regulatory regions that function as transcription start sites or enhancers for neighboring genes (36), which are essential for genetic innovation. However, because of structural similarities between certain TE-derived transcripts and viral genomic sequences, cells could recognize TEs as invading viruses, activate the antiviral innate immune system, and induce cell death (37). This phenomenon has been employed to remove abnormal cells, such as cancer cells. Nevertheless, TE-induced cell death is deleterious to normal cells. When SET domain bifurcated histone lysine methyltransferase 1 (SETDB1) was lost in intestinal stem cells, excessive viral mimicry induced by motivated ERVs triggered ZBP1-dependent necroptosis, which was responsible for inflammatory bowel disease (20). Therefore, the tight control of TEs is critical for promoting genetic innovation, guarding mammalian genome integrity, and preserving cell identity (36, 38). Due to the detrimental effects of TEs, the genome has evolved different ways to repress TEs, such as epigenetic regulation. DNA methylation, H4K20me3, and H3K9me3 have been shown to regulate TEs, respectively, and concurrently (39–41). Our study provided the experimental evidence that H4K20me1 and H4K20me3 marked TEs extensively in TSCs and decreased levels of PR-SET7-H4K20me1/3 resulted in increased expression of ERVs, suggesting H4K20me1 and H4K20me3 are essential, at least to a large extent, for the repression of ERVs in TSCs. Recent work reported that DNMT1 recognizes H4K20me3 via the BAH1 domain to promote DNMT1 deposition on chromatin (19), demonstrating the potential cooperation between H4K20me3 and DNA methylation in silencing TEs resident in the mammalian genome, and this might be the same case in TSCs. In addition, how PR-SET7-mediated H4K20me1 interacts with other histone modifications, such as H3K9me3, to repress ERVs in TSCs needs further investigation.

Previous studies have shown that PR-SET7 acts as a transcriptional repressor or an activator through H4K20me1 (12, 42). In liver-specific *Pr-set7*-KO mice, lower levels of PR-SET7-H4K20me1 accounted for the reduced RNA Pol II release from promoter-proximal pause sites, leading to decreased expression of genes involved in glucose and fatty acid metabolism (43). Recent evidence shows that H4K20me1-mediated enhanced chromatin openness and accessibility could promote the expression of housekeeping genes (13). In current study, we

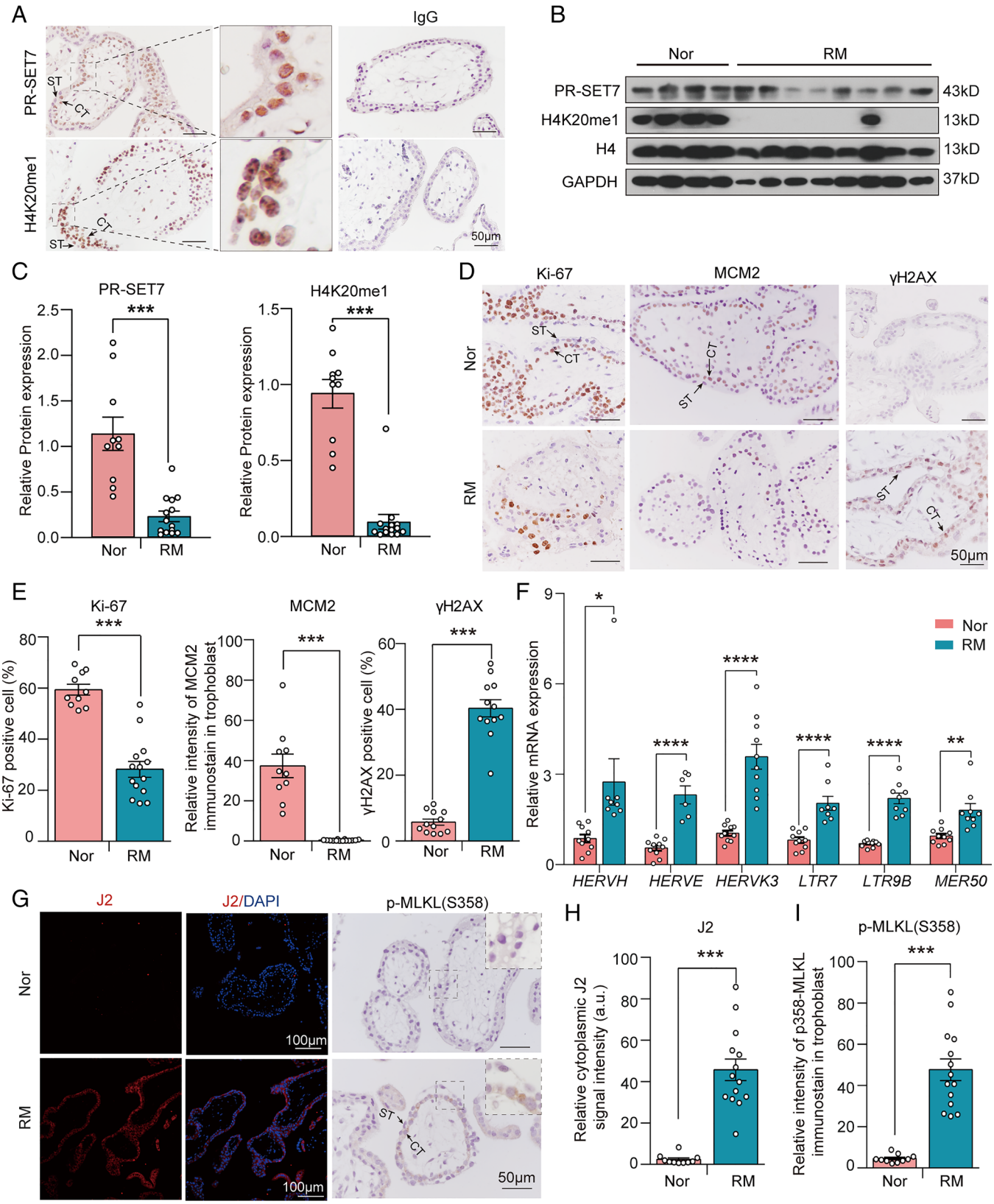

Fig. 7. Decreased expression of PR-SET7 is associated with recurrent miscarriage in humans. (*A*) Immunohistochemical analysis of PR-SET7 and H4K20me1 in the placental villous tissues from normal pregnancies. (*B*) Immunoblot analysis of PR-SET7 and H4K20me1 in the villi from normal and RM pregnancies. Nor, normal control; RM, recurrent miscarriage. GAPDH and H4 were used as loading controls. (*C*) Quantitative results of *B*. (*D*) Immunostaining of Ki-67, MCM2, and γH2AX in the villi from normal and RM pregnancies. (*E*) Quantitative results of *D*. (*F*) qRT-PCR analysis of ERVs in the villi from normal and RM pregnancies. (*G*) Immunostaining analysis of J2 and p-MLKL(S358) in the villi from normal and RM pregnancies. (*H* and *I*) Quantitative results of G. The data shown in *C*, *E*, *F*, *H*, and *I* represent the mean ± SEM. Two-tailed unpaired Student's *t* test, ***$P < 0.001$, ****$P < 0.0001$. n = 10 for Nor, and n = 14 for RM. CT, cytotrophoblast; ST, syncytiotrophoblast.

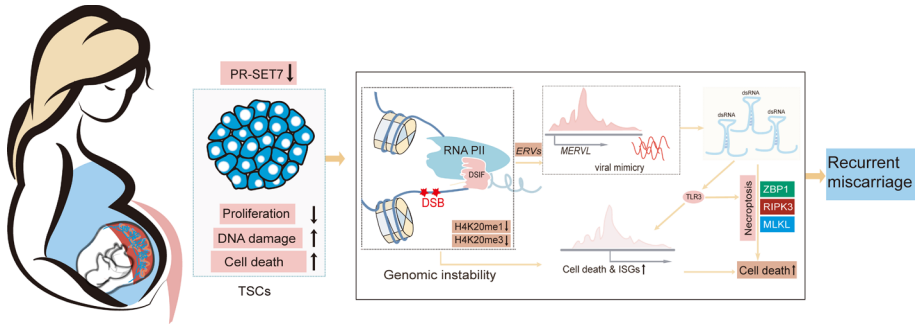

Fig. 8. Schematic illustration showing how PR-SET7 is essential for the survival of trophoblasts. PR-SET7 suppresses interferon response and necroptosis via inhibiting the transcription of ERVs and dsRNA formation. Under a PR-SET7 dysfunctional condition, aberrantly upregulated dsRNAs lead to an overwhelming interferon response and necroptosis, potentially contributing to the pathogenesis of RM.

found that PR-SET7 deficiency leads to cell cycle arrest and significant downregulation of genes associated with cell cycle, suggesting that PR-SET7-H4K20me1 might promote cell cycle progression by activating the transcription of cell cycle-associated genes in trophoblasts. Moreover, it is interesting to note that the H4K20me1 genomic distribution at the gene body in actively transcribed genome areas partially resembles that of H3K36me3 (44). And it has been reported H4K20me1 enrichment in the gene body is positively linked to the ratio of transcriptional elongation (45). This evidence indicates that PR-SET7-H4K20me1 might regulate cell cycle-associated genes via promoting transcriptional elongation in trophoblasts, which merits further investigation.

In essence, our findings achieved in TSCs, clinical biopsies from normal and RM pregnancies, and in vivo trophoblast-specific knock-out mouse models elucidate that PR-SET7 is an epigenetic regulator indispensable for early trophoblast survival and development, and its deficiency triggers the ERVs-dsRNA-interferon pathways and necroptosis, providing insightful information regarding the potential pathophysiological causes of RM.

Materials and Methods

Mice. The *Pr-set7*$^{f/f}$ mice and *Elf5-Cre* transgenic mice were generated as described previously (23, 46). The trophoblast-specific mutant mice were generated by crossing eight-week-old female *Pr-set7*$^{f/f}$ mice with male *Elf5-Cre/Pr-set7*$^{f/+}$ mice, and mice with virginal plus were considered embryonic day 0.5 (E0.5). All the mice were housed in the animal care facility of Xiamen University according to the guidelines for the care and use of laboratory animals. This study was approved by the Animal Care Committee of Xiamen University (XMULAC20170366).

Trophoblast Stem Cell Derivation, Culture, and Transfection. The derivation and maintenance of the *Pr-set7*$^{f/f}$ mTSCs were performed as described previously (47, 48). Briefly, blastocysts from *Pr-set7*$^{f/f}$ pregnant mice were collected at E3.5 and placed in a four-well dish containing mitomycin C-treated mouse embryonic fibroblast (MEF) feeders in TS medium+F4H (RPMI 1640 containing 20% FBS, 2 mM L-glutamine, 1 mM sodium pyruvate, 100 μM β-mercaptoethanol, 25 ng/mL FGF4, and 1 mg/mL Heparin). When blastocyst outgrowth is ready for disaggregation, break the outgrowth with 0.25% trypsin/EDTA, feed the cells with 70% MEF-conditioned medium (MEF-CM), 30% TS medium plus 1.5× FGF4/Heparin for early passages. Maintaining TS cells in a plate coated with Matrigel gel in Serum-Free Culture Medium (Advanced DMEM/F12, 1% Penicillin-streptomycin, 2 mM L-glutamine, 64 mg/L L-ascorbic acid-2-phosphate magnesium, 0.05% BSA, 1 mM sodium pyruvate, 0.5% B27, 1% ITS-supplement, 100 μM β-mercaptoethanol, 25 ng/mL FGF4, and 1 mg/mL Heparin, 2 ng/mL human recombinant TGF-β1) (48). Serum-Free Culture Medium without FGF4, Heparin, and TGF-β1 was used for differentiation experiments.

The derivation, maintenance, and differentiation (STBs and EVT) of hTSCs were performed as described previously (49). CTs were isolated from first trimester placental villi and seeded in a six-well plate coated with Col IV, supplemented with 2 mL of TS medium (DMEM/F12 supplemented with 0.2% FBS, 100 μM β-mercaptoethanol, 0.3% BSA, 1% ITS supplement, 0.05% Penicillin–streptomycin, 1.5 μg/L L-ascorbic acid-2-phosphate magnesium, 50 ng/mL EGF, 0.5 μM A83-01, 2 μM CHIR99021, 1 μM SB431542, 5 μM Y27632, 0.8 mM VPA), and changed the medium every 2 d. The detailed information for chemicals and recombinant proteins used are listed in *SI Appendix*, Table S2.

Human samples collection, histological, and immunostaining analysis, immunoblot analysis, in situ hybridization, siRNA interference, cell proliferation assays, and cell viability assays, RNA extraction, quantitative real-time PCR, J2 pulldown, flow cytometry of cell cycle, RNA-seq and data analysis, ChIP-seq and data analysis, dot blot assay, statistical analysis. Full details can be found in *SI Appendix, Materials and Methods*.

Data, Materials, and Software Availability. All sequencing data, including RNA-seq and ChIP-seq data, has been deposited in the Gene Expression Omnibus database with the accession codes GSE196221, GSE196222, GSE196223, and GSE196224 (50), respectively. All study data are included in the article and/or supporting information.

ACKNOWLEDGMENTS. We thank S. B. Kong and X. W. Lv for their scientific advice. This work was supported in parts by the National Key R&D Program of China (2022YFC2702400 and 2022YFC2704700 to J.L., 2022YFC2702500 and 2021YFC2700302 to H.W.), National Natural Science Foundation of China (82288102 to H.W., 81830045 to D.C., 31971071 and 82171660 to J.L., 82201887 to X.Z., 32000807 to H.C.), Fujian Natural Science Foundation (2020J05006 to H.C.), and Science and Technology Program of Guangzhou, China (202102010006 to D.C.).

Author affiliations: [a]Fujian Provincial Key Laboratory of Reproductive Health Research, Department of Obstetrics and Gynecology, The First Affiliated Hospital of Xiamen University, School of Medicine, Xiamen University, Xiamen, Fujian 361102, China; [b]Department of Obstetrics and Gynecology, The First Affiliated Hospital of Chongqing Medical University, Chongqing 400016, China; [c]Department of Obstetrics and Gynecology, Key Laboratory for Major Obstetric Diseases of Guangdong Province, The Third Affiliated Hospital of Guangzhou Medical University, Guangzhou 510150, China; and [d]Department of Obstetrics and Gynecology, Women and Children's Hospital of Chongqing Medical University, Chongqing 400016, China

Author contributions: X.Z., B.C., H.Q., H.W., and J.L. designed research; X.Z., Y.X., S.R., N.Y., Y.S., Q.Y., Y.Z., H.C., and J.C. performed research; X.Z., W.D., D.C., B.C., H.Q., H.W., and J.L. analyzed data; and X.Z., B.C., H.Q., H.W., and J.L. wrote the paper.

1. E. Dimitriadis, E. Menkhorst, S. Saito, W. H. Kutteh, J. J. Brosens, Recurrent pregnancy loss. *Nat. Rev. Dis. Primers* **6**, 98 (2020).
2. S. Lv *et al.*, The attenuation of trophoblast invasion caused by the downregulation of EZH2 is involved in the pathogenesis of human recurrent miscarriage. *Mol. Ther. Nucleic Acids* **14**, 377–387 (2019).
3. X. H. Wang *et al.*, Low chorionic villous succinate accumulation associates with recurrent spontaneous abortion risk. *Nat. Commun.* **12**, 3428 (2021).
4. B. Saha *et al.*, TEAD4 ensures postimplantation development by promoting trophoblast self-renewal: An implication in early human pregnancy loss. *Proc. Natl. Acad. Sci. U.S.A.* **117**, 17864–17875 (2020).
5. M. Hemberger, C. W. Hanna, W. Dean, Mechanisms of early placental development in mouse and humans. *Nat. Rev. Genet.* **21**, 27–43 (2020).
6. R. Xu, C. Li, X. Liu, S. Gao, Insights into epigenetic patterns in mammalian early embryos. *Protein Cell* **12**, 7–28 (2021).

7. J. Fang *et al.*, Purification and functional characterization of SET8, a nucleosomal histone H4-lysine 20-specific methyltransferase. *Curr. Biol.* **12**, 1086–1099 (2002).
8. K. Nishioka *et al.*, PR-Set7 is a nucleosome-specific methyltransferase that modifies lysine 20 of histone H4 and is associated with silent chromatin. *Mol. Cell* **9**, 1201–1213 (2002).
9. X. Cao *et al.*, Histone H4K20 demethylation by two hHR23 proteins. *Cell Rep.* **30**, 4152–4164.e6 (2020).
10. R. David, Cell cycle: Disposing of SETD8. *Nat. Rev. Mol. Cell Biol.* **11**, 819 (2010).
11. D. B. Beck, H. Oda, S. S. Shen, D. Reinberg, PR-Set7 and H4K20me1: At the crossroads of genome integrity, cell cycle, chromosome condensation, and transcription. *Genes. Dev.* **26**, 325–337 (2012).
12. S. Jørgensen, G. Schotta, C. S. Sørensen, Histone H4 lysine 20 methylation: Key player in epigenetic regulation of genomic integrity. *Nucleic Acids Res.* **41**, 2797–2806 (2013).
13. M. Shoaib *et al.*, Histone H4 lysine 20 mono-methylation directly facilitates chromatin openness and promotes transcription of housekeeping genes. *Nat. Commun.* **12**, 4800 (2021).
14. J. L. Garcia-Perez, T. J. Widmann, I. R. Adams, The impact of transposable elements on mammalian development. *Development* **143**, 4101–4114 (2016).
15. A. G. Diehl, N. Ouyang, A. P. Boyle, Transposable elements contribute to cell and species-specific chromatin looping and gene regulation in mammalian genomes. *Nat. Commun.* **11**, 1796 (2020).
16. J. Y. Lu *et al.*, Homotypic clustering of L1 and B1/Alu repeats compartmentalizes the 3D genome. *Cell Res.* **31**, 613–630 (2021).
17. A. H. Shah *et al.*, The role of human endogenous retroviruses in gliomas: From etiological perspectives and therapeutic implications. *Neuro Oncol.* **23**, 1647–1655 (2021).
18. L. Južnić *et al.*, SETDB1 is required for intestinal epithelial differentiation and the prevention of intestinal inflammation. *Gut* **70**, 485–498 (2021).
19. W. Ren *et al.*, DNMT1 reads heterochromatic H4K20me3 to reinforce LINE-1 DNA methylation. *Nat. Commun.* **12**, 2490 (2021).
20. R. Wang *et al.*, Gut stem cell necroptosis by genome instability triggers bowel inflammation. *Nature* **580**, 386–390 (2020).
21. A. J. Patel *et al.*, PRC2-inactivating mutations in cancer enhance cytotoxic response to DNMT1-targeted therapy via enhanced viral mimicry. *Cancer Discov.* **12**, 2120–2139 (2022).
22. T. Cui *et al.*, PR-Set7 deficiency limits uterine epithelial population growth hampering postnatal gland formation in mice. *Cell Death Differ.* **24**, 2013–2021 (2017).
23. S. Kong *et al.*, Generation of Elf5-Cre knockin mouse strain for trophoblast-specific gene manipulation. *Genesis* **56**, e23101 (2018).
24. C. Yang, K. Wang, Y. Tang Zhou, S. L. Zhang, Histone lysine methyltransferase SET8 is a novel therapeutic target for cancer treatment. *Drug Discov. Today* **26**, 2423–2430 (2021), 10.1016/j.drudis.2021.05.004.
25. A. Iwasaki, P. S. Pillai, Innate immunity to influenza virus infection. *Nat. Rev. Immunol.* **14**, 315–328 (2014).
26. I. Jorgensen, E. A. Miao, Pyroptotic cell death defends against intracellular pathogens. *Immunol. Rev.* **265**, 130–142 (2015).
27. A. G. Snyder, A. Oberst, The antisocial network: Cross talk between cell death programs in host defense. *Annu. Rev. Immunol.* **39**, 77–101 (2021).
28. M. P. Crossley *et al.*, R-loop-derived cytoplasmic RNA-DNA hybrids activate an immune response. *Nature* **613**, 187–194 (2023), 10.1038/s41586-022-05545-9.
29. J. Maelfait, L. Liverpool, J. Rehwinkel, Nucleic acid sensors and programmed cell death. *J. Mol. Biol.* **432**, 552–568 (2020).
30. E. C. Nelissen, A. P. van Montfoort, J. C. Dumoulin, J. L. Evers, Epigenetics and the placenta. *Hum. Reprod. Update* **17**, 397–417 (2011).
31. X. Lv, Z. Cai, S. Li, Increased apoptosis rate of human decidual cells and cytotrophoblasts in patients with recurrent spontaneous abortion as a result of abnormal expression of CDKN1A and Bax. *Exp. Ther. Med.* **12**, 2865–2868 (2016).
32. X. Dong, L. Yang, H. Wang, miR-520 promotes DNA-damage-induced trophoblast cell apoptosis by targeting PARP1 in recurrent spontaneous abortion (RSA). *Gynecol. Endocrinol.* **33**, 274–278 (2017).
33. M. Pasparakis, P. Vandenabeele, Necroptosis and its role in inflammation. *Nature* **517**, 311–320 (2015).
34. N. Robinson *et al.*, Type I interferon induces necroptosis in macrophages during infection with Salmonella enterica serovar Typhimurium. *Nat. Immunol.* **13**, 954–962 (2012).
35. J. Lin *et al.*, RIPK1 counteracts ZBP1-mediated necroptosis to inhibit inflammation. *Nature* **540**, 124–128 (2016).
36. E. B. Chuong, N. C. Elde, C. Feschotte, Regulatory activities of transposable elements: From conflicts to benefits. *Nat. Rev. Genet.* **18**, 71–86 (2017).
37. M. Devos *et al.*, Sensing of endogenous nucleic acids by ZBP1 induces keratinocyte necroptosis and skin inflammation. *J. Exp. Med.* **217**, e20191913 (2020).
38. V. Gorbunova *et al.*, The role of retrotransposable elements in ageing and age-associated diseases. *Nature* **596**, 43–53 (2021).
39. Y. G. Chen, S. Hur, Cellular origins of dsRNA, their recognition and consequences. *Nat. Rev. Mol. Cell Biol.* **23**, 286–301 (2022), 10.1038/s41580-021-00430-1.
40. J. T. Kurup, Z. Han, W. Jin, B. L. Kidder, H4K20me3 methyltransferase SUV420H2 shapes the chromatin landscape of pluripotent embryonic stem cells. *Development* **147**, dev188516 (2020).
41. J. Choi, D. B. Lyons, M. Y. Kim, J. D. Moore, D. Zilberman, Dna methylation and histone H1 jointly repress transposable elements and aberrant intragenic transcripts. *Mol. Cell* **77**, 310–323.e7 (2020).
42. J. Huang *et al.*, Histone lysine methyltransferase Pr-set7/SETD8 promotes neural stem cell reactivation. *EMBO Rep.* **22**, e50994 (2021), 10.15252/embr.202050994.
43. K. C. Nikolaou, P. Moulos, V. Harokopos, G. Chalepakis, I. Talianidis, Kmt5a controls hepatic metabolic pathways by facilitating RNA Pol II release from promoter-proximal regions. *Cell Rep.* **20**, 909–922 (2017).
44. Y. Zhang *et al.*, H3K36 histone methyltransferase Setd2 is required for murine embryonic stem cell differentiation toward endoderm. *Cell Rep.* **8**, 1989–2002 (2014).
45. A. Veloso *et al.*, Rate of elongation by RNA polymerase II is associated with specific gene features and epigenetic modifications. *Genome Res.* **24**, 896–905 (2014).
46. H. Oda *et al.*, Monomethylation of histone H4-lysine 20 is involved in chromosome structure and stability and is essential for mouse development. *Mol. Cell Biol* **29**, 2278–2295 (2009).
47. S. Tanaka, T. Kunath, A. K. Hadjantonakis, A. Nagy, J. Rossant, Promotion of trophoblast stem cell proliferation by FGF4. *Science* **282**, 2072–2075 (1998).
48. C. Kubaczka *et al.*, Derivation and maintenance of murine trophoblast stem cells under defined conditions. *Stem. Cell Rep.* **2**, 232–242 (2014).
49. H. Okae *et al.*, Derivation of human trophoblast stem cells. *Cell Stem. Cell* **22**, 50–63.e6 (2018).
50. J. Lu, ChIP_Seq analysis in cultured hTSCs. NCBI GEO. https://www.ncbi.nlm.nih.gov/geo/query/acc.cgi?acc=GSE196221; ChIP_Seq analysis in cultured mTSC cells with or without Dox. NCBI GEO. https://www.ncbi.nlm.nih.gov/geo/query/acc.cgi?acc=GSE196222; Gene expression in the hTSCs of si-NC and si-PR-SET7 KD hTSCs. NCBI GEO. https://www.ncbi.nlm.nih.gov/geo/query/acc.cgi?acc=GSE196223; Gene expression in the mTSCs of WT and Pr-set7 KO mTSCs. NCBI GEO. https://www.ncbi.nlm.nih.gov/geo/query/acc.cgi?acc=GSE196224. Deposited 6 February 2022.